Impact of the dipole contribution on the terahertz emission of air-based plasma induced by tightly focused femtosecond laser pulses

Alexander P. Shkurinov,[1,2] Anton S. Sinko,[1] Peter M. Solyankin,[1,2] Alexander V. Borodin,[2] Mikhail N. Esaulkov,[2,*] Vladimir V. Annenkov,[3,4] Igor A. Kotelnikov,[3,4] Igor V. Timofeev,[3,4] and Xi-Cheng Zhang[5]

[1]*Department of Physics and International Laser Center, Lomonosov Moscow State University, Leninskie Gory, Moscow 119992, Russia*

[2]*Institute on Laser and Information Technologies of the Russian Academy of Sciences, Branch of the FSRC "Crystallography and Photonics" RAS, Shatura, Moscow Region 140700, Russia*

[3]*Budker Institute of Nuclear Physics SB RAS, Novosibirsk 630090, Russia*

[4]*Novosibirsk State University, Novosibirsk 630090, Russia*

[5]*The Institute of Optics, University of Rochester, Rochester, New York 14627-0186, USA*

(Received 17 January 2017; published 20 April 2017)

The present paper studies the generation mechanism of terahertz (THz) radiation from tightly focused femtosecond laser pulses in a gas medium. We measured the angular radiation pattern under different focusing conditions and observed that, with the deepening of focus, the angular radiation pattern changes and optical-to-THz conversion efficiency increases. The analysis of the observed phenomena led to the assumption that the dipole radiation prevails in most cases despite the existing conception regarding the dominating role of the quadrupole mechanism of radiation. Based on these assumptions, the transient photocurrent theory of the phenomenon presented in this paper was developed by us and used for the numerical fit of the experimental data.

DOI: 10.1103/PhysRevE.95.043209

I. INTRODUCTION

Terahertz (THz) frequency range is one of the remaining scientific gaps in the electromagnetic spectrum with rich potential for scientific research [1]. The generation of THz radiation may occur in a gas medium when it is illuminated by intense femtosecond laser pulses. Initially, THz emission from a gas has always been associated with ionization of the gas, and the emission was thought to be exclusively driven by free electron currents [2,3]. However, the THz radiation generation in air plasma is described nowadays with the assumption that there are two main physical mechanisms which actually take place under certain experimental conditions: four-wave rectification [4–6] and transient photocurrent [7–10] models. The manifestation and predominance of various mechanisms of THz generation depends on several factors: power density of the pump laser beam and whether a "one-color" or a "two-color" experimental scheme is used. In the two-color approach two ultrafast laser fields of fundamental and second harmonic frequencies interact in the gas medium, whereas in the one-color approach only one laser field at fundamental frequency is used for THz wave generation.

In the case of a comparatively weak laser pulse (below the ionizing threshold), the nonlinear properties of the medium are determined by the neutral atoms of the medium [11], which leads to certain phenomena, including THz wave generation [6]. With the increase of the laser intensity, leading to the exceeding of the gas ionization threshold, the second mechanism, which presupposes the radiation of free plasma electrons [12] in the shape of the transient photocurrent [7,13,14], becomes predominant. Assuming the additivity of several physical processes leading to radiation at the same frequency and quite incomplete ionization of gas, all these mechanisms work in laser plasma simultaneously. However, these contributions into the THz signal can be distinguished according to their spectral responses [15].

At the same time, the nonlinear optical signal can be presented in the form of the sum of dipole and quadrupole contributions [16,17] if the nonlinear optical processes lead to the generation of the electromagnetic waves at the same frequency. Attempts to separate these waves date back to the early study of nonlinear optics [18,19]. In THz nonlinear optics the problem of separation of various contributions into the measurable signal is also actual, especially when they are of different origins [15].

In this paper, we study the influence of dipole and quadrupole currents on the THz radiation in the one-color experimental scheme. We carried out experiments on the generation of THz radiation under different focusing conditions, starting with a relatively long focal distance and gradually increasing the focusing depth until a microplasma regime is reached.

In this paper we use the term "filament" for the description of the interaction area with the understanding that the term "filament" usually indicates a particular plasma structure where self-focusing is balanced by plasma diffraction. Nevertheless, in this paper the length of the plasma is always defined by the geometrical focusing of the lens. However, we use the term filament due to the evident unity of the main mechanisms of generation of THz radiation in our case and in the case of "extended filament."

II. EXPERIMENTAL SETUP

In order to justify our assumption, the experiment was carried out with the use of the setup shown in Fig. 1. The laser beam from a Ti:sapphire regenerative amplifier (Spectra Physics SpitFire Pro, 797 nm, 130 fs, pulse energy up to 1.5 mJ, beam diameter up to 1 cm) was focused with one of the lenses into the ambient air. In order to change the length of the filament and its diameter we used a set of lenses

*esaulkov_mich@mail.ru

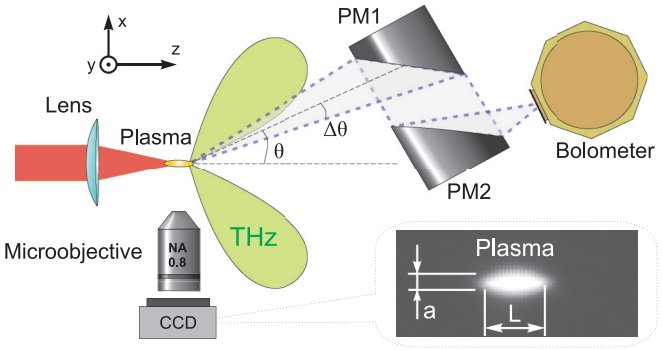

FIG. 1. Schematic presentation of the experimental setup used to study the angular radiation pattern (top view): a laser beam is focused with a lens into ambient air. A pair of off-axis parabolic mirrors (PM1, PM2) positioned at angle θ from the optical beam axis collimates and refocuses the THz radiation into the window of the Si bolometer. The angle θ can be continuously varied in the range $[-90^\circ, 90^\circ]$.

having different focal distances: plano-convex lenses from fused silica with focal distances of 100, 50, 40, 25, and 7 mm and an aspherical acrylic lens, CAY046 (Thorlabs, Inc.), with an effective focal distance of 4.6 mm. A pair of Glan prisms and an iris aperture were used to manage and control the pulse energy in the interaction area and the laser beam diameter. The polarization of the optical beam was kept linear and horizontal.

To estimate the dimensions of the filaments we analyzed the images of the plasma cloud appearing in the focal region. We collected images of the plasma fluorescence using a CoolSNAP Color (Roper Scientific) CCD camera with a microscope objective. Fluorescence bands of nitrogen and nitrogen ions (N_2 and N_2^+) which lie around 350–450 nm [20] contributed most to the observed filament image.

The collection system of THz radiation included a pair of off-axis parabolic mirrors (PM1 and PM2, 50.6 mm in diameter), an effective focal distance of 101.2 mm, and a helium-cooled silicon bolometer (Infrared Laboratories general purpose 4.2 K bolometer). For studying the angular radiation pattern, the collection system was mounted on a rotation stage which could be rotated about the vertical axis which passes through the focal point of the lens. The detection angle θ between the optical beam axis and the first parabolic mirror PM1 could be varied in the range -90° to $+90^\circ$ where 0° corresponds to the propagation direction of the laser beam. The geometry of the setup does not allow us to study the THz radiation intensity in the backward direction, i.e., at the detection angles beyond $+90^\circ$ and -90°. The polarization of the THz radiation could be studied with the help of a wire-grid THz polarizer placed between PM1 and PM2.

In this experiment, the multistage filtration system of THz radiation was utilized in order to prevent the influence of radiation of other spectral ranges. A 2.4-mm-thick Teflon filter (transmission coefficient 0.85 over the THz spectral range of our study) was placed before the first parabolic mirror to scatter the pump radiation. Two 0.35-mm silicon wafers (10 Ω cm, boron doping, transmission coefficient of each wafer was 0.42 for normal incidence) were attached to the bolometer window. The input window of the bolometer was made from 1-mm-thick high-density polyethylene (HDPE) (transmission coefficient 0.9). For complete separation of the THz signal, a 0.8-mm crystalline quartz filter with garnet powder was installed inside the bolometer and cooled to 4 K (transmission coefficient below 3 THz is 0.8, at higher frequencies the filter is nontransparent), which limits the range under study to 0–3 THz. As we estimated from spectral measurements using a Michelson interferometer, most of the energy of THz radiation is concentrated in this spectral interval, which is also consistent with the results described in Ref. [21]. The total transmission coefficient of our filtering system in the range of 0.1–3 THz was approximately 0.1, while beyond this spectral range we estimate the transmission to be lower than 10^{-4}.

III. RESULTS OF THE MEASUREMENTS

For each lens with a different focal length we used a fixed optical beam aperture (7 mm) and maximum available pulse energy (700 μJ). The only exceptions were the acrylic lens with a focal distance of 4.6 mm (the aperture of the lens itself was 3.7 mm and the maximum pulse energy below the damage threshold was approximately 250 μJ) and the lens with a focal distance of 7 mm (maximum pulse energy was chosen to be 450 μJ to avoid optical damage). For all focusing conditions, we studied the dependence of the intensity of the THz radiation on the detection angle θ. Due to the fact that the first parabolic mirror has a limited aperture, it could collect only a part of the radiation emitted into large angles from the optical axis. This led to the dependence of the radiation collection efficiency on the value of the emission angle, which has to be taken into consideration when processing experimental data. This procedure is described in Sec. A of this paper.

The results of our measurements are shown in Fig. 3 with dots. It is clearly seen that for all focusing conditions, the in-plane angular radiation pattern contains two lobes of approximately equal intensity, which corresponds to the conical profile of the THz radiation. For all focusing conditions and linear polarization of the optical beam, we did not observe the dependence of the spatial profile of the THz radiation on the direction of the optical pulse polarization. Note that the radiation distribution shown in Fig. 3 is not fully symmetric in θ. This effect was revealed only after numerical processing of the results of measurements. We suppose that this is because the central axis of our measuring system was slightly misaligned from the axis of the plasma channel.

To measure the polarization of the THz radiation, we set the detector angle θ equal to the direction of the maximum of THz intensity (θ_{max}) and then rotated the THz polarizer placed between PM1 and PM2. In both lobes we observed maximum THz intensity when the polarizer orientation was horizontal. For vertical orientation of the polarizer, the THz intensity was from 10 to 50 times lower for the longest and shortest focal distances of the lenses, respectively. We observed a similar result when the polarization of the optical beam was changed to vertical linear. Our measurements agree with the earlier published studies [22] on the properties of radial polarization of the THz beam.

Due to the fact that the detector moves only in the horizontal plane and its aperture is limited, some amount of the THz radiation leaving the generator at large angles with respect to the horizontal plane cannot reach the bolometer since it will miss the aperture of the first parabolic mirror (PM1).

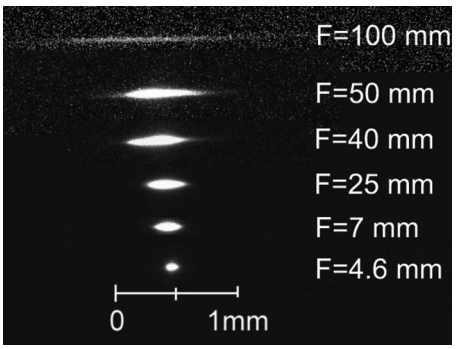

FIG. 2. Side view CCD images of photo-induced plasma fluorescence taken under different focusing conditions. Measured length L and radii a of the filaments are indicated in Table I.

Therefore we measured only part of the whole radiation pattern which was spread near the horizontal plane. That is why when we studied the radially polarized THz beam with conical spatial structure we saw only its part which was having linear horizontal polarization.

As we move towards shorter focal lengths of the lenses, the filament length becomes shorter (see Fig. 2), and the angle of maximum THz intensity $\theta_{\max}$ gets larger (see Figs. 3 and 4).

To compare the optical-to-THz conversion efficiency for different focusing conditions, we integrate the THz signal intensity over the emission angle from -90° to 90°. Here we take into account that the measured THz energy at large detection angles θ is only a part of the total energy

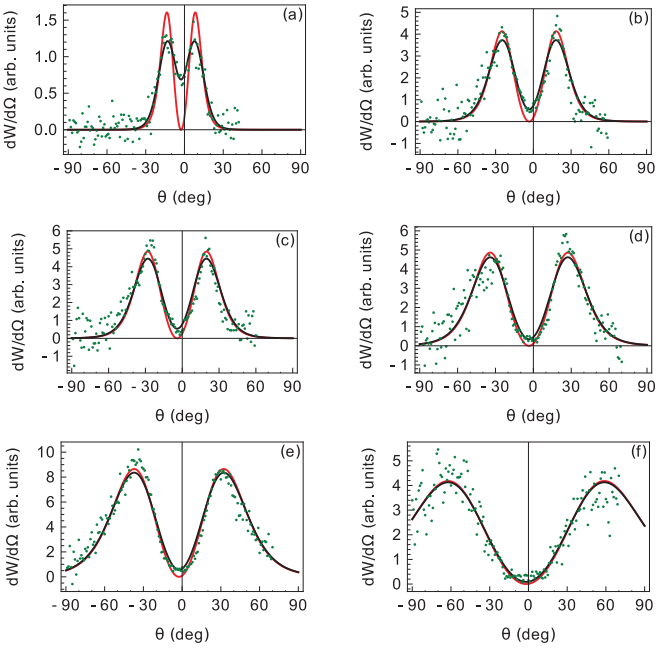

FIG. 3. Measurements of angular distribution $dW/d\Omega$ of THz radiation for different focusing conditions (green dots), theoretical fit [red (gray) line]), and theoretical fit corrected by instrumental function (black line); focal lengths F are indicated on the plots (see Table I for the parameters of the fit): (a) $F = 100$ mm, (b) $F = 50$ mm, (c) $F = 40$ mm, (d) $F = 25$ mm, (e) $F = 7$ mm, and (f) $F = 4.6$ mm.

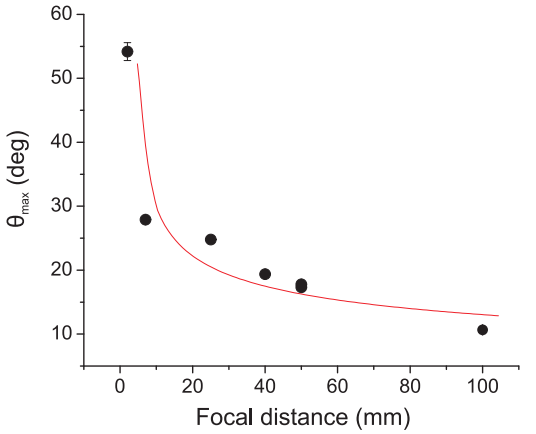

FIG. 4. Angle $\theta_{\max}$ for which the maximum of the THz intensity is observed vs focal length.

emitted into that angle due to the finite aperture of the parabolic mirror, so we need to multiply the raw data by a correction coefficient depending on the detection angle θ before the integration procedure. The procedure of calculating the correction coefficient is described in Appendix B. After that, we take as a figure-of-merit the integrated THz intensity divided by the optical pulse energy. The black circles in Fig. 5 show the resulting conversion efficiency versus the focal distance of the lens. It is clearly seen that, for the smallest focal distances, THz generation becomes more efficient. The smaller focusing radii F leads to increase in the peak laser intensity and plasma density [23] and sharpening of the field intensity gradients. As we see from our results, the efficiency of optical-to-THz energy conversion also increases, despite that the length and the volume of the plasma channel decrease for the deep focusing case. Therefore we conclude that the influence of decrease in the plasma dimensions plays an inferior role in the optical-to THz conversion. Nevertheless, it becomes harder to collect all the emitted energy since the angle of the maximum emitted intensity $\theta_{\max}$ can reach 55° (see Fig. 4).

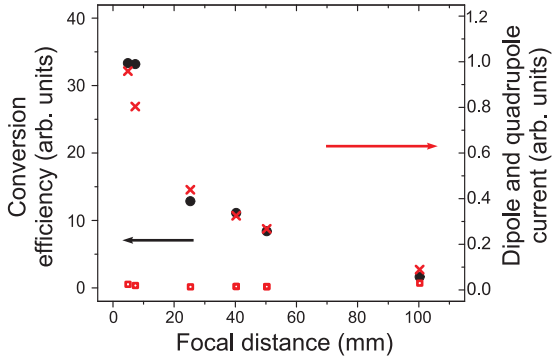

FIG. 5. Black circles: Efficiency of the optical-to-THz energy conversion versus focal length. Red crosses: Contribution of the dipole current to the THz signal. Red boxes: Contribution of the quadrupole current to the THz signal.

IV. A MODEL OF THZ RADIATION

Previous phenomenological treatments of the problem of radiation from the plasma filament induced by a powerful laser pulse, such as Refs. [14,24–27], did not take into consideration quantitative selection between the dipole and quadrupole mechanisms of generation of the THz radiation. Here we consider contributions of both dipole and quadrupole currents inside the filament.

To extend the existing models we imagine that the current density $\mathbf{j} = \mathbf{j}(\mathbf{x},t)$ induced in the filament by the pump laser pulse is already computed as a solution of the equations derived in Refs. [28,29] or evaluated with the help of a Particle-In-Cell (PIC) code. The Fourier transform $\mathbf{j}_\omega = \int_{-\infty}^{\infty} \mathbf{j}(\mathbf{x},t)e^{i\omega t}dt$ of the current is related to the radiated magnetic field in the wave zone through the integral

$$\mathbf{B}_\omega(\mathbf{r}) = ik\mathbf{n}\frac{e^{ikr}}{cr}\int d^3x'\,\mathbf{j}_\omega(\mathbf{x}')e^{-ik\mathbf{n}\cdot\mathbf{x}'}, \tag{1}$$

where $\mathbf{n} = \mathbf{r}/r$ and $k = \omega/c$ (see Eqs. (9.13) and (9.39) in Ref. [30]). The integral can be evaluated in an analytic form for two models of the current density profiles presented below. The difference between the two models will be clarified hereafter. Based on our PIC simulations (to be published elsewhere) and for the sake of simplicity we assume that the vector $\mathbf{j}$ has only the z component and consider two profiles, namely:

$$j_z^{(1)}(x,y,z,t) = j_1\frac{(z-ct)}{c\tau}\exp\left(-\frac{x^2+y^2}{a^2} - \frac{(z-ct)^2}{c^2\tau^2} - \frac{z^2}{L^2}\right), \tag{2a}$$

$$j_z^{(2)}(x,y,z,t) = j_2\frac{\partial}{\partial z}\left[(z-ct)\exp\left(-\frac{x^2+y^2}{a^2} - \frac{(z-ct)^2}{c^2\tau^2} - \frac{z^2}{L^2}\right)\right]. \tag{2b}$$

The functions $j_z^{(1)}$ and $j_z^{(2)}$ simulate a pump laser pulse with the radius a and the length $c\tau$ propagating through a filament with the length L; the amplitudes j_1 and j_2 as well as the lengths L and a are varied below when finding the numerical fitting shown in Fig. 3. To justify this approach, we note that the authors of Ref. [31] also assumed the THz radiation to originate from the longitudinal electron current, whereas the often-discussed wake oscillations at the plasma frequency do not strongly contribute to the THz emission spectrum. The spacial profiles of the currents given by Eq. (2) roughly approximate those found in our preliminary numerical simulation.

The ponderomotive force of the pump laser pulse produces a longitudinal current structure, which propagates with approximately the speed of light [22,31]. The interference of radiation from distinct points along the propagation axis leads to a conical emission. This mechanism of THz radiation is often referred to as the transition-Cherenkov mechanism, although the classic Cherenkov radiation requires the source moving at superluminal velocity, which is not the case under consideration.

The principal difference of the profile given by Eq. (2a) from Eq. (2b) is characterized by the value of $\int_{-\infty}^{\infty} j_z dz$, which is nonzero in the case of the dipolar type of charge distribution in the medium and zero in the case of higher orders of charge distribution. The condition $\int \mathbf{j}(\mathbf{x},t)d^3x = 0$, which holds for $j_z^{(2)}$ but not for $j_z^{(1)}$, means that the dipole moment of the system is permanently zero. Thus, $j_z^{(1)}$ is responsible for the dipole radiation, whereas $j_z^{(2)}$ is responsible for the quadrupole one. The type of the radiation is also seen from the corresponding expressions for the magnetic field radiated by currents $j_z^{(1)}$ and $j_z^{(2)}$ and observed at the point with coordinates $\mathbf{r}$ at time t in the time domain. Due to axial symmetry, the magnetic field has only the azimuthal α component:

$$B_\alpha^{(1)} = \frac{\pi^{1/2}}{c^2 r}I_1 L\Delta\omega^3\tau^2(2\Delta\omega^2 t'^2 - 1)e^{-\Delta\omega^2 t'^2}\sin(\theta), \tag{3a}$$

$$B_\alpha^{(2)} = \frac{\pi^{1/2}}{c^2 r}I_2 L\Delta\omega^4\tau^3(2\Delta\omega^2 t'^2 - 3)\Delta\omega t' e^{-\Delta\omega^2 t'^2}\sin(2\theta). \tag{3b}$$

Here $I_1 = \pi a^2 j_1$ and $I_2 = \pi a^2 j_2$ are the total currents, $t' = t - r/c$ is the retarded time,

$$\Delta\omega = \frac{c}{\sqrt{c^2\tau^2 + a^2\sin^2\theta + L^2(1-\cos\theta)^2}} \tag{4}$$

is the spectral width of the radiation, and θ is the angle between the filament axis and the direction to the radiation detector. In the case of a short filament ($L \to 0$) the dipole field (3a) varies with θ as $\sin(\theta)$, whereas the quadrupole field (3b) is proportional to $\sin(2\theta)$. Note that the frequency spectrum of the field is determined by the pump pulse duration τ, the total length of the filament L, and the angle of observation θ. The duration of the radiated (THz) pulse is roughly evaluated as $T = 1/\Delta\omega$. In the forward direction ($\theta = 0$) it coincides with the pump pulse duration τ. It reaches maximal value $T \approx L/c$ for the pulse radiated at the right angle to the filament axis. The total energy

$$\frac{dW}{d\Omega} = r^2\int_{-\infty}^{\infty}\frac{B^2}{4\pi}dt$$

radiated into a given solid angle $d\Omega = \sin\theta d\theta d\alpha$ can also be calculated in a closed form. As is seen from the result of the calculation

$$\frac{dW}{d\Omega} = \frac{3\pi^{3/2}}{16\sqrt{2}}c^2L^2\Delta\omega^5\tau^4\left[I_1^2 + 5I_2^2\Delta\omega^2\tau^2\cos^2\theta\right]\sin^2\theta, \tag{5}$$

the $j_z^{(2)}$ current does not interfere with $j_z^{(1)}$ (as there is no term proportional to $I_1 I_2$). We believe that the absence of the interference is not a typical case since an instant value of B^2 does contain the product $I_1 I_2$ but it disappears after integration over time.

Angular patterns predicted by Eq. (5) are shown in Fig. 6 for a selected set of parameters such that only either I_1 or I_2 is nonzero. The dipole and quadrupole angular patterns are visually different in the case of a short filament. If $L/c\tau \lesssim 0.4$ the quadrupole pattern has two visible backward lobes, whereas the dipole pattern always has only two forward lobes. The backward lobes become too small in the case of a long filament with $L/c\tau \gtrsim 1$. The width of the forward lobes and the angle $\theta_{\max}$ at which the maximum radiation intensity is

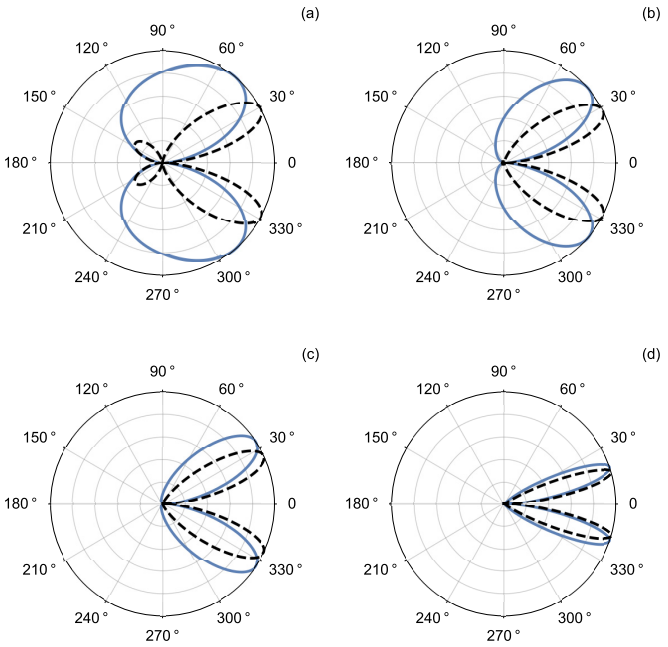

FIG. 6. Angular patterns of $dW/d\Omega$ normalized over their maximums for $a = c\tau$ and various ratios $L/c\tau$: (a) 0.4, (b) 1, (c) 2, and (d) 8. Solid blue line: dipole radiation due to I_1. Black dashed line: quadrupole radiation due to I_2.

reached for quadrupole radiation are smaller than those for the dipole one at equal values of $L/c\tau$.

Moreover, the intensity of THz radiation resulting from the quadrupole current is zero in the direction orthogonal to the laser beam axis, i.e., at $\theta = 90^\circ$ and -90° for any values of $L/c\tau$. The dipole and quadrupole angular patterns become actually indistinguishable if $L/c\tau \gtrsim 8$.

For the optical pulse with duration $\tau = 130$ fs as in the reported experiment, the spacial length of the pump laser pulse is $c\tau \approx 39$ μm, which roughly leads to the experimentally measured values of the ratio $L/c\tau \gtrsim 1$ of the length of the plasma fluorescence pattern shown in Fig. 2 to the value of $c\tau$. As shown in Table I the experimental and fitted values of $L/c\tau$ coincide within a factor of 2–3, showing the same tendency as in the case when the focus length F varies.

For a large ratio $L/c\tau$ the opening angle of the radiation cone scales as $\theta_{\max} \approx \sqrt{c\tau/L}$ for both the dipole and

TABLE I. Experimental and fit parameters of the filaments; the values of L and a are normalized over the laser pulse length $c\tau$, which under our experimental conditions was equal to 39 μm.

	Experiment		Fit No. 1			Fit No. 2		
F (mm)	L	a	I_1	I_2	L	I_1	I_2	L
100	61.5	4.3	0.71	0.13	24.71	0.00	0.53	16.72
50	16.7	2.6	2.14	0.01	6.99	0.00	1.37	4.87
40	18.0	3.1	2.60	0.01	5.62	0.00	1.73	3.82
25	12.1	3.5	3.51	0.00	3.32	0.00	3.61	1.58
7	9.7	6.7	6.43	0.05	2.34	0.00	5.22	1.22
4.6	4.1	4.8	7.67	0.09	0.76	0.00	22.55	0.17

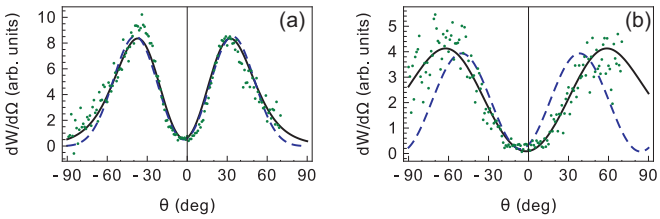

FIG. 7. Comparison of experimentally measured total energy dW radiated in solid angle $d\Omega$ with the numerical fits: No. 1 (solid line) and No. 2 (dashed line) for focal lengths $F = 7$ mm (a) and $F = 4.6$ mm (b).

quadrupole patterns. Returning to Eq. (4), one can see that $T \approx 2\tau$ for the THz radiation propagating at the angle $\theta_{\max}$.

V. NUMERICAL FIT

Equations (5) were used to fit experimental data as shown in Fig. 3. At first we tried to approximate the data with the function (5) by assuming both a quadrupole nature and a dipole nature of the emitting current, i.e., by varying I_1, I_2, L, and a. When computing numerical fits, we took into account the response function of our detection system as a two-dimensional Gaussian profile with the width $\Delta\theta = 6^\circ$ as described in SecAppendix A.

The result is presented in Table I as Fit No. 1. It reveals significant domination of the dipole current even at large focus length F when the filament length L is so large that the dipole and quadrupole radiation are hardly distinguishable. As seen in Table. I, the quadrupole current I_2 is small as compared to the dipole current I_1. We conclude therefore that

$$\frac{dW}{d\Omega} \approx \frac{3\pi^{3/2}}{16\sqrt{2}} c^2 L^2 \Delta\omega^5 \tau^4 I_1^2 \sin^2\theta. \tag{6}$$

We then repeated the fitting procedure with the dipole current forcibly set to zero. The result is presented in Table I as Fit No. 2. By comparing the residuals for the two fits we conclude that Fit No. 1 is better for any F even though the plots for Fit No. 2 are visually indistinguishable at large F from the corresponding plots for Fit No. 1 in Fig. 3. The most significant difference is observed at small F as shown in Fig. 7 for $F = 7$ mm and $F = 4.6$ mm.

We also plot the results of the fits normalized to unity in Fig. 5 along with the energy conversion efficiency. As we see from the graph, the contribution of the dipole current increases as the focusing distance decreases while the quadrupole contribution is small and its value remains on approximately the same level for all focusing conditions.

As we see from the results of the fits, the computed dimensions of the THz emitter are smaller than the visible dimensions of the filament. This means that most of the THz radiation is generated in the thin part of the plasma where the plasma density is close to the critical value for THz radiation. The inner part of the plasma is not transparent for THz radiation, and the outer layers of plasma have much lower electron density so that their contribution into the observed signal is also lower. Also, the dimensions of the plasma cloud, if measured using the CCD, are most likely overestimated due to expansion of the plasma after passing of the optical

pulse. We observed the same phenomena in filaments formed in the gas cluster medium where the dimensions of the nonlinear medium emitting THz waves may be measured also by observing the x-ray radiation from the clusters [32].

VI. CONCLUSIONS

In order to clarify the nature of THz radiation which occurs in the case of deep focusing of laser radiation in a one-color experimental scheme, we compared the contributions of dipole and quadrupole currents taking place in plasma. We discovered that the dominating contribution can be determined on the basis of the analysis of spatial distribution of THz radiation intensity. Besides, the radiation caused by the quadrupole current under deep focusing leads to narrower peaks in the angular distribution of THz radiation intensity compared to the radiation caused by the dipole current. The quadruple photocurrent is also characterized by zero value of THz radiation intensity in the direction orthogonal to the laser pulse propagation axis, and the presence of petals of the radiation propagation, which are directed backwards, are not characteristic for the dipole photocurrent. Moreover, the present paper studies the development of the theoretical dependence of the measured duration and spectral width of THz pulse on the observation angle—detection angle θ [see Eq. (4)]. As we see from our experimental results and the theoretical fits, the spatial profile and the energy of the THz emission is mostly defined by the contribution of the longitudinal dipole current but not the quadrupole one for all focusing conditions under study. The part of the plasma cloud which contributes to the observed THz radiation is shorter than the visible filament length measured with the help of a CCD camera. The efficiency of optical-to-THz energy conversion increases as well as the amount of the dipole contribution for the case of deep focusing of the laser radiation.

ACKNOWLEDGMENTS

We appreciate useful comments on this work from Dr. Fabrizio Buccheri and Kang Liu. This work was supported by the Russian Federation President Grant for Leading Scientific Schools (Grant No. NSh-9695.2016.2) and by the Russian Foundation for Basic Research (Grants No. 15-32-20966, No. 15-32-20961, and No. 14-22-01098 and partially Grants No. 16-32-60171, No. 16-02-01217, and No. 16-29-11800). X.-C. Zhang's research was also sponsored by the Army Research Office and was accomplished under Grant Number W911NF-16-1-0436. The views and conclusions contained in this document are those of the authors and should not be interpreted as representing the official policies, either expressed or implied, of the Army Research Office or the U.S. Government. The U.S. Government is authorized to reproduce and distribute reprints for Government purposes notwithstanding any copyright notation herein.

APPENDIX A: RESPONSE FUNCTION

We assume that a theory allows us to calculate the angular distribution of THz radiation in the form

$$\frac{dW}{d\Omega} = f(\theta), \tag{A1}$$

where $f(\theta)$ is given, e.g., by the right-hand side of Eq. (5). Then the angular distribution which takes into account the instrumental response function $h(\theta,\theta')$ is determined by

$$\left(\frac{dW}{d\Omega}\right)_h = \int_0^\pi h(\theta,\theta')\, f(\theta') d\theta'. \tag{A2}$$

To find $h(\theta,\theta')$, we take into account that the measured signal from the cone-shaped angular distribution is collected with the help of an aperture of the first parabolic mirror PM1. We consider here that each point of the detector parabolic mirror PM1 corresponds to a single point of a round "detector window" placed at the distance r (equal to the focal distance of PM1). We write the Cartesian coordinates $\{x,y,z\}$ of an arbitrary point on the detector window via the spherical coordinates $\{r,\alpha,\theta\}$ with the origin at the point of the laser focus:

$$\{x,y,z\} = \{r\sin\theta\cos\alpha, r\sin\theta\sin\alpha, r\cos\theta\}.$$

The square of the distance between two such points (on the detector window) with the coordinates $\{r,\alpha,\theta\}$ and $\{r,\alpha',\theta'\}$ is

$$l^2 = 2r^2[1 - \cos\theta\cos\theta' - \sin\theta\sin\theta'\cos(\alpha-\alpha')],$$

so that

$$\left(\frac{dW}{d\Omega}\right)_h = \int_0^\pi d\theta' \sin(\theta') \int_{-\pi}^{\pi} d\alpha' h_2(\{\theta,\alpha\},\{\theta',\alpha'\})\, f(\theta'), \tag{A3}$$

where h_2 is a two-dimensional instrumental response function. We approximate it by the Gaussian distribution

$$h_2(\{\theta,\alpha\},\{\theta',\alpha'\}) = \frac{A}{\pi\Delta\theta^2}\exp\left[-\frac{l^2}{r^2\Delta\theta^2}\right]. \tag{A4}$$

The integration over α' in Eq. (A3) can be done in a closed form. Comparing the result with Eq. (A2) we find the one-dimensional instrumental response function:

$$h(\theta,\theta') = \frac{2A\sin(\theta')}{\Delta\theta^2} e^{-2(1-\cos\theta\cos\theta')/\Delta\theta^2} I_0\left(\frac{2\sin\theta\sin\theta'}{\Delta\theta^2}\right), \tag{A5}$$

where I_0 denotes the Bessel function. In the case of $2\sin\theta\sin\theta' \gg \Delta\theta^2$, this expression transforms to

$$h(\theta,\theta') = \frac{A\sqrt{\sin\theta'}}{\sqrt{\pi}\Delta\theta\sqrt{\sin\theta}} \mathrm{e}^{-4\sin^2(\frac{\theta-\theta'}{2})/\Delta\theta^2}.$$

The constant A is determined from the condition

$$\int_0^\pi d\theta' h(\theta,\theta') = 1$$

and is equal to

$$A = \frac{1}{1-e^{-4/\Delta\theta^2}} \approx 1.$$

We took $\Delta\theta = 6^\circ$, which provides the best numerical fit to the angular diagrams in the case of long filaments.

APPENDIX B: CORRECTION MULTIPLIER

Let R be the effective focusing distance of the first parabolic mirror. The effective aperture of the first parabolic mirror in the detection system (PM1) can be represented as a circle

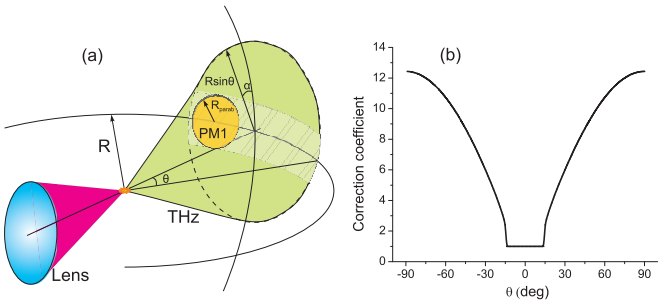

FIG. 8. (a) Scheme showing the decrease in efficiency of THz radiation collection for wide emission cones. (b) Values of the correction coefficient for the experimental parameters used.

with radius R_{parab} moving along a circle with radius R in the horizontal plane and collecting radiation from a part of the "detection sphere" with radius R when we rotate the detection system (see Fig. 8). Let us assume that in the focal point of the parabolic mirror we have a source of THz radiation emitting in a narrow cone with cone angle θ and a very narrow angular width ($\Delta\theta \approx 0$) and a homogeneous distribution over the azimuth angle α. Emission from this source crosses the "detection sphere" with radius R along a circle with radius $R\sin\theta$. It is clear that, if $R\sin\theta > R_{\text{parab}}$, part of the emitted radiation will miss the detector at any orientation θ_{detect} of the detector (in Fig. 8, only the radiation shown by the dashed lines can be collected by the detector). In order to calculate the value of the correction coefficient by which the obtained signal should be multiplied in order to compare the energy efficiency of the THz generation, we need to find the ratio of the length of the whole circle along which the THz radiation crosses the "detection sphere" ($2\pi R\sin\theta$) and the length of its part that gets into the dashed area of the sphere. In the case of a wide THz direction cone, when $R\sin\theta > R_{\text{parab}}$, the aperture of the detector positioned at the angle θ collects only part of the emitted energy. For the narrow cone of THz radiation, when $R\sin\theta < R_{\text{parab}}$, the detector collects all the emitted energy and therefore the correction multiplier equals 1. The values of the correction coefficient as a function of the emission angle θ for the sizes and focusing distance of the parabolic mirror used in the experiment are given in the Fig. 8 with the scheme clarifying the idea.

[1] X.-C. Zhang, A. Shkurinov, and Y. Zhang, Nat. Photonics **11**, 16 (2017).
[2] G. A. Askaryan, Sov. Phys. JETP **15**, 943 (1962).
[3] H. Hamster, A. Sullivan, S. Gordon, W. White, and R. W. Falcone, Phys. Rev. Lett. **71**, 2725 (1993).
[4] M. Kreß, T. Löffler, M. D. Thomson, R. Dörner, H. Gimpel, K. Zrost, T. Ergler, R. Moshammer, U. Morgner, J. Ullrich, and H. G. Roskos, Opt. Lett. **29**, 1120 (2004).
[5] J. Dai, X. Xie, and X.-C. Zhang, Phys. Rev. Lett. **97**, 103903 (2006).
[6] D. J. Cook and R. M. Hochstrasser, Opt. Lett. **25**, 1210 (2000).
[7] K. Y. Kim, J. H. Glownia, A. J. Taylor, and G. Rodriguez, Opt. Express **15**, 4577 (2007).
[8] I. Babushkin, W. Kuehn, C. Köhler, S. Skupin, L. Bergé, K. Reimann, M. Woerner, J. Herrmann, and T. Elsaesser, Phys. Rev. Lett. **105**, 053903 (2010).
[9] V. A. Andreeva, O. G. Kosareva, N. A. Panov, D. E. Shipilo, P. M. Solyankin, M. N. Esaulkov, P. González de Alaiza Martínez, A. P. Shkurinov, V. A. Makarov, L. Bergé, and S. L. Chin, Phys. Rev. Lett. **116**, 063902 (2016).
[10] M. Clerici, M. Peccianti, B. E. Schmidt, L. Caspani, M. Shalaby, M. Giguère, A. Lotti, A. Couairon, F. Légaré, T. Ozaki, D. Faccio, and R. Morandotti, Phys. Rev. Lett. **110**, 253901 (2013).
[11] R. W. Boyd, *Nonlinear Optics*, 2nd ed. (Academic, London, 1992).
[12] H. Hamster, A. Sullivan, S. Gordon, and R. W. Falcone, Phys. Rev. E **49**, 671 (1994).
[13] C.-C. Cheng, E. M. Wright, and J. V. Moloney, Phys. Rev. Lett. **87**, 213001 (2001).
[14] A. V. Balakin, A. V. Borodin, I. A. Kotelnikov, and A. P. Shkurinov, J. Opt. Soc. Am. B **27**, 16 (2010).
[15] A. V. Borodin, N. A. Panov, O. G. Kosareva, V. A. Andreeva, M. N. Esaulkov, V. A. Makarov, A. P. Shkurinov, S. L. Chin, and X.-C. Zhang, Opt. Lett. **38**, 1906 (2013).
[16] N. I. Koroteev, Sov. Phys. Usp. **30**, 628 (1987).
[17] A. P. Shkurinov, A. V. Dubrovskii, and N. I. Koroteev, Phys. Rev. Lett. **70**, 1085 (1993).
[18] N. Bloembergen, R. K. Chang, S. S. Jha, and C. H. Lee, Phys. Rev. **174**, 813 (1968).
[19] E. Adler, Phys. Rev. **134**, A728 (1964).
[20] A. Talebpour, M. Abdel-Fattah, A. Bandrauk, and S. Chin, Laser Phys. **11**, 68 (2001).
[21] F. Buccheri and X.-C. Zhang, Optica **2**, 366 (2015).
[22] C. D. Amico, A. Houard, S. Akturk, Y. Liu, J. L. Bloas, M. Franco, B. Prade, A. Couairon, V. T. Tikhonchuk, and A. Mysyrowicz, New J. Phys. **10**, 013015 (2008).
[23] F. Théberge, W. Liu, P. T. Simard, A. Becker, and S. L. Chin, Phys. Rev. E **74**, 036406 (2006).
[24] J. Zheng, C. X. Yu, Z. J. Zheng, and K. A. Tanaka, Phys. Plasmas **12**, 093105 (2005).
[25] C. D'Amico, A. Houard, M. Franco, B. Prade, A. Mysyrowicz, A. Couairon, and V. T. Tikhonchuk, Phys. Rev. Lett. **98**, 235002 (2007).
[26] N. A. Panov, O. G. Kosareva, V. A. Andreeva, A. B. Savel'ev, D. S. Uryupina, R. V. Volkov, V. A. Makarov, and A. P. Shkurinov, JETP Lett. **93**, 638 (2011).
[27] F. Jahangiri, M. Hashida, S. Tokita, T. Nagashima, M. Hangyo, and S. Sakabe, Appl. Phys. Lett. **102**, 191106 (2013).
[28] L. M. Gorbunov, P. Mora, and T. M. Antonsen, Phys. Plasmas **4**, 4358 (1997).
[29] H.-C. Wu, J. Meyer-ter-Vehn, H. Ruhl, and Z.-M. Sheng, Phys. Rev. E **83**, 036407 (2011).

[30] J. D. Jackson, *Classical Electrodynamics*, 3rd ed. (Wiley & Sons, New York, 1999).

[31] I. Thiele, R. Nuter, B. Bousquet, V. Tikhonchuk, S. Skupin, X. Davoine, L. Gremillet, and L. Bergé, Phys. Rev. E **94**, 063202 (2016).

[32] A. V. Balakin, M. S. Dzhidzhoev, V. M. Gordienko, M. N. Esaulkov, I. A. Zhvaniya, K. A. Ivanov, I. A. Kotelnikov, N. A. Kuzechkin, I. A. Ozheredov, V. Y. Panchenko, A. B. Savel'ev, M. B. Smirnov, P. M. Solyankin, and A. P. Shkurinov, IEEE Trans. Terahertz Sci. Technol. **7**, 70 (2017).